Available online at www.sciencedirect.com

ScienceDirect

Physics Procedia 50 (2013) 150 – 155

Physics Procedia

International Federation for Heat Treatment and Surface Engineering 20th Congress
Beijing, China, 23-25 October 2012

Influences of Y addition on mechanical properties and oxidation resistance of CrN coating

Z.T. Wu[a], Z.B. Qi[b], F.P. Zhu[a], B. Liu[a], Z.C. Wang[a,*]

[a]*College of Chemistry and Chemical Engineering, Xiamen University, Xiamen 361005, China*
[b]*College of Materials Science and Engineering, Xiamen University of Technology, Xiamen 361005, China*

Abstract

$Cr_{1-x}Y_xN$ coatings were fabricated by reactive co-sputtering deposition and the Y content was changed by varying the Y target power. The influence of varying amounts of Y addition on the mechanical properties and oxidation resistance of CrN coatings has been studied. The results reveal that Y ions substitute Cr ions in Cr-N lattice forming the solid solution $Cr_{1-x}Y_xN$ coatings. Y doping has a beneficial effect on the improvements of hardness and adhesion of the coatings. After the oxidation in air at 850℃ for 2 h, The CrN coating with 1.2 at. % Y addition exhibits superior oxidation resistance than Y-free CrN coating, while over doping of Y produces detrimental effects on oxidation resistance of the coatings.

Keywords: CrN coating; co-sputtering deposition; structure; adhesion; oxidation resistance.

1. Main text Introduction

Chromium nitride (CrN) coatings have been proposed to be a promising hard coating material owing to its high hardness, wear, corrosion and high temperature oxidation resistance [1-3]. Compared with TiN coating, which has been widely used as hard and wear-resistant coatings in engineering, CrN coating has higher hardness, better corrosion resistance and oxidation resistance even at 700℃ [4, 5]. Adding a third element is an effective method to further improve the mechanical properties and oxidation resistance of the CrN coatings, such as doping V [6], Si [7, 8] and Al [9, 10] to form nanocomposite or single-phase (solid solution) coatings, while the influences of Y addition

* Corresponding author. Tel.: +86-592-2180738; fax: +86-592-2180738.
*E-mail address:*zcwang@xmu.edu.cn

doi:10.1016/j.phpro.2013.11.025

by reactive co-sputtering deposition on structure, mechanical properties and oxidation resistance of CrN coatings are still rarely involved. The aim of this work was to obtain detailed information about these influences.

2. Experimental details

$Cr_{1-x}Y_xN$ coatings were deposited on polished silicon wafers (used for SEM observation) and WC alloy substrates (used for nanoindentation and scratch tests) by reactive co-sputtering deposition technique in an Ar and N_2 atmosphere (99.999% purity). Both Cr target (Ø 76 × 5 mm, 99.99% purity) and Y target (Ø 76 × 5 mm, 99.99% purity) were used. During the deposition, the working pressure was kept at 0.30 Pa with nitrogen flow percentage $N_2/(N_2+Ar)$ fixed at 20%. The Cr target power (DC, AE) was adjusted to 250W, while the Y target power (RF, AE) was set as 0W, 50W, 100W and 150W, respectively. The deposition temperature was 300℃. No bias was applied to the substrates.

Coating thickness was measured by Dektak3 profilometer (VEECO, USA). The thickness of Cr-Y-N coatings was almost maintained at ~ 1.85 μm. Chemical compositions of the coatings were determined by electron probe microanalysis (EPMA, JXA-8100, Japan). Crystal structure of the coatings was investigated by Panalytical X'pert PRO X-ray diffraction (XRD, Philips, Netherlands) using Cu k_α radiation as X-ray source. The cross-sectional morphologies of the coatings were observed by SEM (Leo 1530, Germany). Nanoindentation (CSM Instrument SA, Switzerland) was performed to determine the coating hardness using Oliver-Pharr techniques [11]. The penetration depth was controlled about 10% of the coatings' thickness (~ 185 nm) in order to eliminate the influence of substrates. The adhesion between substrate and coating was determined by a scratch tester (CSM Instrument SA, Switzerland) with a Rockwell C diamond tip (Ø 100 μm) using a linearly increasing load from 0.9 N to 50 N with loading rate of 98.2 N/min. The oxidation were conducted in air at 850℃ for 2 h. The oxidation resistance of the Cr-Y-N coatings was characterized by the method of measuring thickness of the oxide scales.

3. Results and Discussion

3.1. Chemical composition and phase structure

The chemical compositions of the Cr-Y-N coatings with respect to different Y target power are plotted in Table 1. The Y/(Y+Cr) atomic ratio monotonously increases with improving the Y target power, while the N/(Y+Cr) atomic ratio remains constant at ~ 90.8 at. %. With the values of the calculated Y/(Y+Cr) atomic ratio of the Cr-Y-N coatings, we defined our coatings as CrN, $Cr_{0.997}Y_{0.003}N$, $Cr_{0.988}Y_{0.012}N$ and $Cr_{0.978}Y_{0.022}N$, in accordance with the chemical compositions of the coatings, revealed by EPMA analyses.

Table 1.T he chemical compositions of the Cr-Y-N coatings with respect to Y target power.

Y target power (W)	0	50	100	150
N/(Y+Cr) (atomic ratio)	90.2%	89.5%	91.6%	92.0%
Y/(Y+Cr) (atomic ratio)	0.0%	0.3%	1.2%	2.2%

Fig .1 illustrates the XRD patterns of the $Cr_{1-x}Y_xN$ coatings. All the coatings exhibit a single phase *fcc* structure similar with CrN (JCPDS 76-2494). The $Cr_{1-x}Y_xN$ coatings are identified as cubic structure, where Y was dissolved in Cr-N to form solid solution. The (1 1 1), (3 1 1) and (2 2 2) peaks of $Cr_{1-x}Y_xN$ coatings shift to lower angles with increasing Y content, implying an increase in lattice parameters. The peaks shifting can be explained by the substitution of Cr ions by Y ions. Since the ionic radius of Y^{3+} (89 pm) is larger than Cr^{3+} (69 pm), the crystal lattice will expand after the substitution of Cr^{3+} by Y^{3+}. Thus, the diffraction angles will shift to lower values according to the Bragg law.

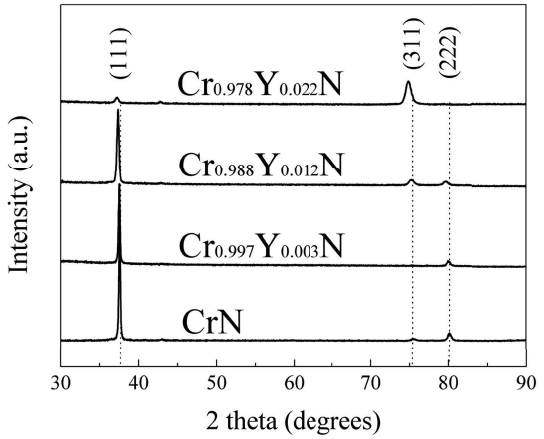

Fig. 1. The XRD patterns of the $Cr_{1-x}Y_xN$ coatings.

Another obvious observation is that the preferred orientations of $Cr_{1-x}Y_xN$ coatings gradually change from (111) to (311) with increasing Y content. The mechanisms for textural evolution in films have been explained so far from the viewpoints of thermodynamics and kinetics. Thompson [12] has proposed that both surface and strain energy minimizations govern the grain growth in thin films. Thus the competition between both energies influences the texture in polycrystalline thin films. If the (hkl) has the lowest surface energy, and hence, a (hkl) preferred orientation should appear under a low stress condition since the surface energy in this case has a dominant contribution to the total free energy for the system. It has been demonstrated [13] that the Gibbs free energy is orientation dependent in all crystal systems in stress fields which are not purely hydrostatic, and a preferred orientation arises as a result of the synthesis of materials under a high stress condition in which an elastic strain energy contribution will be dominant. If a biaxial stress is considered, in the case of the cubic system, the Gibbs free energy of the crystal per unit volume, due to the strain energy, can be given by [13, 14]:

$$G^{fcc} = G_0^{fcc} - \frac{1}{2}\times\sigma^2\times\left[s_{11} - 2\left(s_{11} - s_{12} - \frac{1}{2}s_{44}\right)\times\left(\sigma_1'\sigma_2' + \sigma_2'\sigma_3' + \sigma_1'\sigma_3'\right)\right] \quad (1)$$

Where G_0^{fcc} is the Gibbs free energy of the system under zero stress, σ is the magnitude of the stress, s_{ij} (i, j = 1, 2, 4) is the elastic compliance tensor and σ_i (i = 1, 2, 3) is the component of the rotated stress. Hence, if (hkl) is normal to the stress plane, G^{fcc} will reach the minimum under the high stress condition, in which the strain energy is dominant, compared with the surface energy. So the (311) preferred orientation arises with increasing Y content may be attributed to the formation of a high stress field caused by the solid solution effects.

3.2. Hardness and adhesion

Hardness and adhesion of $Cr_{1-x}Y_xN$ coatings as a function of Y content were measured by nanoindentation and revetest scratch tester, respectively. As can be seen in Fig. 2 (a), the indentation hardness monotonously increases from 12.9 ± 0.5 GPa for CrN to 13.7 ± 0.4 GPa for $Cr_{0.978}Y_{0.022}N$. The improvement of hardness is attributed to the solid solution effect. The scratch tests show that Y doping also has a beneficial effect on the adhesion of the coatings, as presented in Fig. 2 (b). All the coatings exhibit similar scratch failure modes, starting with chips spallation on the side of the tracks, and then wedge spallation, and finally substrate exposure. The chips and wedge spallation are the common failure modes for hard coatings and related to the adhesion [15]. Therefore, the critical load (L_c) corresponding to the first spallation occurring (marked by the black arrow) is used to represent the adhesion between the substrate and the coating during the tests. The critical loads of $Cr_{1-x}Y_xN$ (x=0.002, 0.012 and 0.022) coatings are about 4.3 ± 0.3 N, while 2.5 ± 0.3 N for CrN coating. The reactive element Y can getter the residual contaminations

on the substrates effectively and lead to the improvement of adhesion [16].

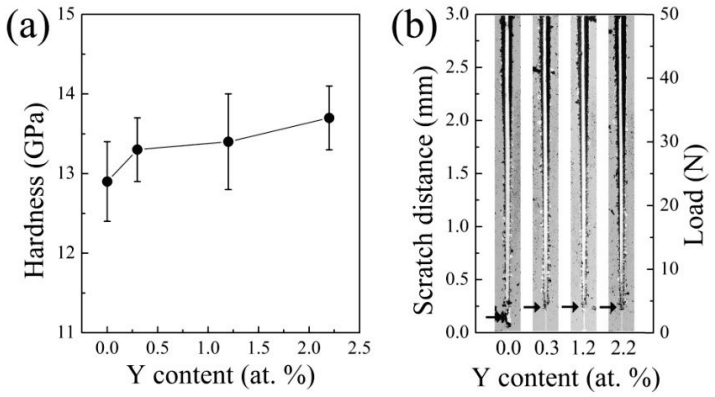

Fig. 2. Hardness (a) and the panorama scratch tracks of the $Cr_{1-x}Y_xN$ coatings (b).

3.3. Oxidation resistance

The glancing angle x-ray diffraction (GAXRD) patterns of the $Cr_{1-x}Y_xN$ coatings after oxidation are exhibited in Fig. 3. The Cr_2O_3 (JCPDS 38-1479) peaks show up after oxidation at 850℃. The Cr_2O_3 peaks are not obvious for the $Cr_{1-x}Y_xN$ (0.003 and 0.012) coatings. Correspondingly, both the intensities of Cr_2O_3 (012) and (011) peaks of $Cr_{0.978}Y_{0.022}N$ coating are greater than $Cr_{1-x}Y_xN$ (x=0.003 and 0.012) coatings, it means that more Cr_2O_3 scales formed on $Cr_{0.978}Y_{0.022}N$ coating during the oxidation. Therefore, the oxidation resistance of $Cr_{1-x}Y_xN$ (x=0.003 and 0.012) coatings should be better than $Cr_{0.978}Y_{0.022}N$ coating, agreeing well with the actual results of SEM observation, as shown in Fig. 4. After the oxidation, the nitride coatings still keep the dense columnar structure. However, the oxide scales exhibit undefined structure with rough surface. The oxide scale thickness is ~ 310 nm for CrN, ~ 240 nm for $Cr_{0.997}Y_{0.003}N$, ~ 190 nm for $Cr_{0.988}Y_{0.012}N$ and ~ 370 nm for $Cr_{0.978}Y_{0.022}N$. The result reveal that Y addition with appropriate amounts can improve the oxidation resistance of CrN coatings, while over doping of Y produces detrimental effects on the coatings.

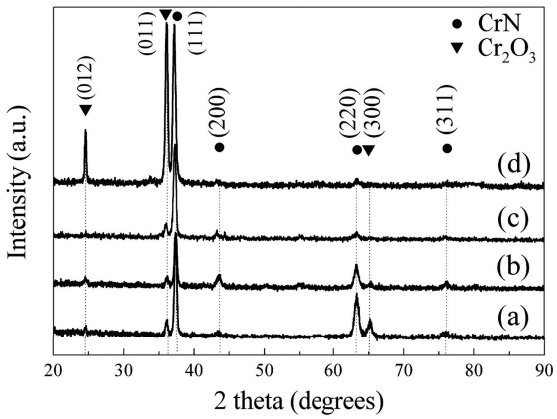

Fig. 3. The GAXRD patterns of the $Cr_{1-x}Y_xN$ coatings after oxidation at 850℃ in air for 2 h. (a) CrN coating, (b) $Cr_{0.997}Y_{0.003}N$ coating, (c) $Cr_{0.988}Y_{0.012}N$ coating, (d) $Cr_{0.978}Y_{0.022}N$ coating.

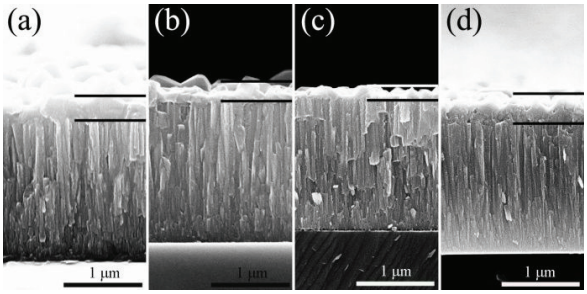

Fig. 4. The Cross-sectional SEM images of $Cr_{1-x}Y_xN$ coatings after oxidation at 850℃ in air for 2 h. (a) CrN coating, (b) $Cr_{0.997}Y_{0.003}N$ coating, (c) $Cr_{0.988}Y_{0.012}N$ coating, (d) $Cr_{0.978}Y_{0.022}N$ coating.

The improvement of oxidation resistance is associated with the reactive elements effect [17, 18]. During oxidation, the reactive element ions outward diffused and segregated to scale grain boundaries or scale interface reducing the oxide growth rate and enhancing scale adhesion. But the oxidation resistance of $Cr_{0.978}Y_{0.022}N$ coating is worse than CrN coating, over doping of reactive element produces detrimental effects. The reason maybe: excess reactive element in the coatings can form a second phase oxide or intermetallic, when incorporated into the oxide, these oxides allow for fast oxygen transport, thus increase the scale thickness [19, 20]. Over doping of reactive element can also promote internal oxidation, hence reduce the scale adhesion. If too much reactive element is incorporated into the oxide scales, reactive element oxide particles can form on oxide grain boundaries. These particles again can allow faster oxygen transport, thus increase the scale growth rate.

4. Conclusions

The $Cr_{1-x}Y_xN$ coatings were deposited by reactive co-sputtering deposition to explore the influence of varying amounts of Y addition on mechanical properties and oxidation resistance. All the coatings exhibit a single phase *fcc* structure. The Y doping has a beneficial impact on the improvements of hardness the adhesion of the $Cr_{1-x}Y_xN$ coatings. During the scratch tests, all the coatings exhibit similar failure modes, chips and wedge spallation. The CrN coating with 1.2 at. % Y addition shows the best oxidation resistance. However, over doping of Y produces detrimental effect on oxidation resistance of the coatings, it is probably attributed to the formation of a second phase oxide or reactive element oxide particles.

Acknowledgements

The authors thank for the financial support from the Science and Technology Foundation of Fujian (2012H6019) and Xiamen (3502Z20113003), the National Key Technology R&D Program of China (2007BAE05B04).

References

[1] G. Bertrand, C. Savall, C. Meunier, Properties of reactively RF magnetron-sputtered chromium nitride coatings, Surface and Coatings Technology, 96 (1997) 323-329.
[2] D. Lee, Y. Lee, S. Kwon, High temperature oxidation of a CrN coating deposited on a steel substrate by ion plating, Surface and Coatings Technology, 141 (2001) 227-231.
[3] Z. Han, J. Tian, Q. Lai, X. Yu, G. Li, Effect of N_2 partial pressure on the microstructure and mechanical properties of magnetron sputtered CrN_x, Surface and Coatings Technology, 162 (2003) 189-193.
[4] M. Lembke, D. Lewis, W.-D. Münz, Localised oxidation defects in TiAlN/CrN superlattice structured hard coatings grown by cathodic arc/unbalanced magnetron deposition on various substrate materials, Surface and Coatings Technology, 125 (2000) 263-268.
[5] Y. Otani, S. Hofmann, High temperature oxidation behaviour of $(Ti_{1-x}Cr_x)$ N coatings, Thin solid films, 287 (1996) 188-192.
[6] M. Uchida, N. Nihira, A. Mitsuo, K. Toyoda, K. Kubota, T. Aizawa, Friction and wear properties of CrAlN and CrVN films deposited by cathodic arc ion plating method, Surface and Coatings Technology, 177 (2004) 627-630.
[7] G. Kim, B. Kim, S. Lee, High-speed wear behaviors of CrSiN coatings for the industrial applications of water hydraulics, Surface and Coatings Technology, 200 (2005) 1814-1818.

[8] H. Lee, W. Jung, J. Han, S. Seo, J. Kim, Y. Bae, The synthesis of CrSiN film deposited using magnetron sputtering system, Surface and Coatings Technology, 200 (2005) 1026-1030.
[9] H.C. Barshilia, N. Selvakumar, B. Deepthi, K. Rajam, A comparative study of reactive direct current magnetron sputtered CrAlN and CrN coatings, Surface and Coatings Technology, 201 (2006) 2193-2201.
[10] X.-Z. Ding, X. Zeng, Structural, mechanical and tribological properties of CrAlN coatings deposited by reactive unbalanced magnetron sputtering, Surface and Coatings Technology, 200 (2005) 1372-1376.
[11] W.C. Oliver, G.M. Pharr, Improved technique for determining hardness and elastic modulus using load and displacement sensing indentation experiments, Journal of materials research, 7 (1992) 1564-1583.
[12] C. Thompson, Structure evolution during processing of polycrystalline films, Annual review of materials science, 30 (2000) 159-190.
[13] D. McKenzie, M. Bilek, Electron diffraction from polycrystalline materials showing stress induced preferred orientation, Journal of Applied Physics, 86 (1999) 230-236.
[14] D. McKenzie, M. Bilek, Thermodynamic theory for preferred orientation in materials prepared by energetic condensation, Thin solid films, 382 (2001) 280-287.
[15] S. Bull, E. Berasetegui, An overview of the potential of quantitative coating adhesion measurement by scratch testing, Tribology International, 39 (2006) 99-114.
[16] A. Jones, A. McCabe, S. Bull, G. Dearnaley, The effects of deposition temperature and interlayer thickness on the adhesion of ion-assisted titanium nitride films produced with yttrium metal interlayers, Nuclear Instruments and Methods in Physics Research Section B: Beam Interactions with Materials and Atoms, 80 (1993) 1397-1401.
[17] F. Rovere, P.H. Mayrhofer, Impact of yttrium on structure and mechanical properties of Cr–Al–N thin films, Journal of Vacuum Science & Technology A: Vacuum, Surfaces, and Films, 25 (2007) 1336-1340.
[18] R. Braun, F. Rovere, P. Mayrhofer, C. Leyens, Environmental protection of γ-TiAl based alloy Ti-45Al-8Nb by CrAlYN thin films and thermal barrier coatings, Intermetallics, 18 (2010) 479-486.
[19] J. Stringer, B. Wilcox, R. Jaffee, The high-temperature oxidation of nickel-20 wt.% chromium alloys containing dispersed oxide phases, Oxidation of metals, 5 (1972) 11-47.
[20] C. Cotell, G. Yurek, R. Hussey, D. Mitchell, M. Graham, The influence of grain-boundary segregation of Y in Cr_2O_3 on the oxidation of Cr metal, Oxidation of metals, 34 (1990) 173-200.